Design and Experimental Validation of Closed-Form CBF-Based Safe Control for Stewart Platform Under Multiple Constraints

Benedictus C. G. Cinun[1,2] Tua A. Tamba[2] Immanuel R. Santjoko[2] Xiaofeng Wang[3] Bin Hu[1,4]

***Abstract*— This paper presents a closed-form solution of a Control Barrier Function (CBF) formulation for ensuring safety in the operation of a Stewart platform prototype. The proposed controller simultaneously enforces position and velocity constraints, using an energy-based CBF for position safety and a standard CBF for velocity safety. Instead of solving the associated safety Quadratic Program (QP) at each control step, an explicit closed-form solution is derived to compute the safe control inputs, significantly reducing computational cost and enabling real-time implementation. Simulation results demonstrate that the closed-form and QP-based methods yield identical control actions and successfully guarantee safe operation. Experimental validation on the developed prototype further confirms the suitability of the closed-form approach for real-time deployment in safety-critical parallel robotic systems.**

***Keywords*—closed-form solution, Control Barrier Function, Stewart platform prototype, Experimental validation**

I. Introduction

Safety is a fundamental requirement in engineering and robotics, ensuring that systems operate within predefined constraints [1]. Control Barrier Functions (CBFs) provide a formal framework for enforcing such constraints by modifying control inputs in real time [1]. However, practical implementation faces three main challenges: (i) defining valid CBFs for high-relative-degree constraints [2], (ii) handling multiple simultaneous safety constraints [3], and (iii) reducing the computation time of real-time Quadratic Programming (QP) solvers [4], [5].

Several approaches have been developed to address the high-relative-degree problem. Exponential CBFs (ECBFs) [6] overcome this challenge for position-based safety constraints by introducing auxiliary dynamics that ensure exponential convergence toward the safe set. High-Order CBFs (HOCBFs) [7] generalize ECBFs by allowing more flexible, nonlinear class-$\mathcal{K}$ functions, enabling broader applicability and finer tuning of conservativeness. An alternative strategy is to apply a reduced-order model for CBF design, though this can introduce divergence from the behavior of the full-order system [8]. More recently, energy-based CBFs [9], [10] incorporate kinetic energy into the barrier function, effectively reducing the relative degree of second-order robotic systems to one and simplifying the constraint formulation. For enforcing multiple constraints, composition methods such as the Log-Sum-Exp (LSE) approximation [3], [11], [12] provide smooth, differentiable $\min/\max$ operations.

While these methods address formulation challenges, real-time applicability drives interest in closed-form solutions. Closed-form CBF solutions replace online QP solving with explicit analytical expressions, avoiding high computational cost and potential feasibility issues. This method reduces computation time and handles multiple constraints, with applications in trajectory tracking [4] and multi-agent coordination under disturbances and uncertainties [5]. A usage of closed-form safety control has also been implemented for a nonlinear system that utilized output-feedback controller [13]. The LSE approximation has proven to be effective for data-driven controllers, including reinforcement learning, by eliminating solving QP in each step while preserving safety guarantees [14]. Neural network (NN)-based controllers can similarly benefit from closed-form safety filters that rapidly project unsafe outputs into the safe set [15]. Recent extensions also incorporate input constraints [16] and multi-constraint composition techniques [12], [17], further broadening applicability. Although many closed-form techniques are currently being explored, by the time of writing this paper, there is no literature that explores the closed-form solution that not only enforce multiple constraints, but also enforces different types of CBF formulations.

Among various robotic platforms, the Stewart platform is an especially relevant testbed for closed-form CBF controllers, with no prior experimental demonstrations on parallel mechanisms. This six-degree-of-freedom (6-DoF) parallel manipulator offers higher payload capacity, stiffness, and motion precision compared to its serial counterparts [18]. Its versatility has supported applications ranging from flight simulation and marine wave compensation [19], [20] to surgical platforms [21] and astronomical instrumentation [22], [23]. At the same time, its nonlinear coupling and strict workspace limits present significant challenges for safety-critical control, making it an ideal platform for evaluating CBF formulations.

Despite the progress in closed-form CBF methods, to the best of our knowledge no prior work unifies different CBF formulations, such as energy-based and velocity-based CBF, into a single closed-form controller, nor experimentally

[1] B. C. G. Cinun is with the Department of Electrical and Computer Engineering at University of Houston, Houston, TX 77004, USA. (e-mail: bgerodacinun@uh.edu

[2] T. A. Tamba and I. R. Santjoko are with the Department of Electrical Engineering, Parahyangan Catholic University, Bandung 40141, West Java, Indonesia (ttamba@unpar.ac.id, 6152001008@student.unpar.ac.id)

[3] X. Wang is with Department of Electrical Engineering, University of South Carolina, Columbia, SC 29208, USA (email.....)

[1,4]B. Hu is with Department of Engineering Technology, Electrical and Computer Engineering, University of Houston, Houston, TX 77004, USA (bhu11@central.uh.edu)

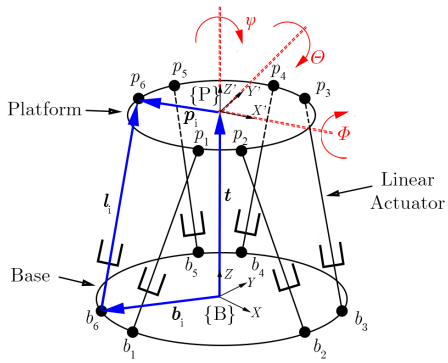

(a)

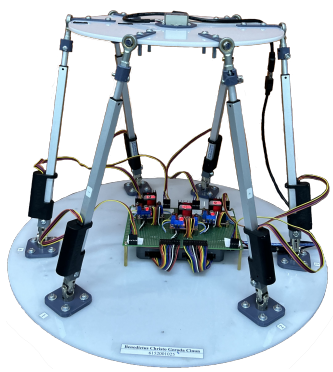

(b)

Fig. 1. (a) The schematic of Stewart platform and (b) the developed prototype.

validates such an approach on a parallel manipulator like the Stewart platform.

In this work, we propose and experimentally validate a closed-form CBF controller for a Stewart platform that simultaneously enforces multiple position and velocity safety constraints. The method integrates different CBF types within a unified analytical control law and employs a modified Log-Sum-Exp (LSE) approximation to enable adjustable conservativeness across constraints. By eliminating the need for online optimization, the approach achieves computational efficiency suitable for real-time implementation on safety-critical robotic systems.

II. Preliminaries

This section will present the fundamental theories that were defined in many previous research, which includes the kinematic and dynamics analysis of the Stewart platform and technical details of the CBF formulation.

A. Stewart Platform Kinematics, Dynamics and Control

The kinematic model of the Stewart platform in this paper is based on the schematic shown in Fig. 1(a). The system consists of three main components: a fixed base with a global frame $\{\mathrm{B}\}$, a moving platform with a body frame $\{\mathrm{P}\}$, and six linear actuators connecting them. The base attachment points are denoted by joints b_i, and the platform attachment points by joints p_i, for $i = 1, \ldots, 6$. This setup allows six degrees of freedom (DoF) for the platform: three translational and three rotational motions with respect to the X, Y, and Z axes.

Let $\vec{t} = [X', Y', Z']^{\mathrm{T}}$ denote the platform's position and $\vec{r} = [\phi, \theta, \psi]^{\mathrm{T}}$ its orientation, both relative to the base frame $\{\mathrm{B}\}$. The generalized coordinate of the system is defined as $q = \left[\vec{t}, \vec{r}\right]^{\mathrm{T}}$. Let $\vec{b}_i$ and $\vec{p}_i$ be the positions of joints b_i and p_i, respectively, expressed in $\{\mathrm{B}\}$. The vector from b_i to p_i, denoted $\vec{l}_i$, can be computed by [24]:

$$\vec{l}_i = \vec{t} + \mathrm{R}\vec{p}_i - \vec{b}_i \tag{1}$$

where $\mathrm{R} \in \mathrm{SO}(3)$ is the 3D rotation matrix corresponding to the Euler angles $\vec{r}$. Given the platform pose q, the actuator lengths $\|\vec{l}_i\|$ can be directly computed via (1).

The dynamic model of the Stewart platform is derived by decomposing the system into two main components: the legs and the platform. The leg dynamics are obtained using the Euler-Lagrange formulation, while the platform dynamics are derived using the Newton-Euler formulation, as described in [24]. By combining these models, the overall dynamics of the Stewart platform in task-space can be expressed in the following general form:

$$\mathrm{M}(q)\ddot{q} + \mathrm{C}(q, \dot{q})\dot{q} + \mathrm{G}(q) = \mathrm{H}(q)\mathrm{F} \tag{2}$$

where $\mathrm{M}(q)$ is the inertial matrix, $\mathrm{C}(q, \dot{q})$ represents the Coriolis and centrifugal terms, $\mathrm{G}(q)$ is the gravity vector, $\mathrm{H}(q)$ is the inverse-transposed Jacobian matrix, and F is the vector of actuator forces. The details of the derivation are omitted in this paper, but can be seen in detail through [24]–[26]. The result of the derivation converge to the same general structure shown in (2).

The Stewart platform is controlled via full-state feedback linearization, which cancels nonlinearities in the dynamic model and transforms the system into a linear, decoupled form. The control law is:

$$u = -K\left(\begin{bmatrix} q \\ \dot{q} \end{bmatrix} - \begin{bmatrix} q_{des} \\ \dot{q}_{des} \end{bmatrix}\right) \tag{3}$$

where K is the feedback control gains, q and $\dot{q}$ are the current platform position and velocity, while q_{des} and $\dot{q}_{des}$ are the desired platform states. The control input u is mapped to desired actuator forces by $\mathrm{F}_{des} = \mathrm{H}^{-1}\{\mathrm{M}u + \mathrm{C}\dot{q} + \mathrm{G}\}$ Then, F_{des} is used as the control input for the dynamic model defined in (2). The details of the developed low-cost Stewart platform prototype are shown in [].

B. Control Barrier Function

Consider a nonlinear affine control system defined as:

$$\dot{x} = f(x) + g(x)u \tag{4}$$

where $x \in D \subset \mathbb{R}^n$ is the state vector, and $u \in U \subseteq \mathbb{R}^m$ is the control input. In control theory, safety is typically defined as the requirement that system trajectories remain within a predefined safe set S [1], [10]. This set is commonly expressed as:

$$\begin{aligned} S &= \{x \in \mathbb{R}^n : h(x) \geq 0\} \\ \partial S &= \{x \in \mathbb{R}^n : h(x) = 0\} \\ \mathrm{Int}(S) &= \{x \in \mathbb{R}^n : h(x) > 0\} \end{aligned} \tag{5}$$

where $h : D \subset \mathbb{R}^n \to \mathbb{R}$ is a continuously differentiable function.

Definition 1. *A function $h(x)$ is called a CBF if there exists an extended class-$\mathcal{K}$ function α such that the following inequality is satisfied for all $x \in S$ [1]:*

$$\sup_{u \in U} \{\underbrace{L_f h(x) + Lgh(x)u}_{\dot{h}(x,u)}\} \geq -\alpha(h(x)) \tag{6}$$

where $L_f h(x) = \nabla h(x) f(x)$ and $L_g h(x) = \nabla h(x) g(x)$. A common choice is the linear function $\alpha(h) = \alpha h$, where $\alpha > 0$ is a gain that defines the trade-off between safety enforcement and performance. Larger values of α allow more relaxed constraint enforcement, while smaller values enforce safety more aggressively.

This standard CBF condition applies when $h(x)$ has *relative-degree one*, meaning that the control input u appears in the first time derivative of $h(x)$. However, systems with second-order dynamics, such as the Stewart platform, require a higher-order CBF formulation, since the control input appears only after differentiating $h(x)$ twice [1], [6]. In contrast, the velocity-based constraints are inherently relative-degree one and thus admit the original first-order CBF condition.

C. Energy-Based CBF

An approach to address the relative-degree problem is the Energy-Based CBF, which reformulates the safety constraint of a second-order system to possess relative-degree one. This formulation incorporates the system's kinetic energy into the safety function, allowing velocity terms to be included into the constraint. As a result, the first-time derivative of the function naturally yields acceleration-level terms that include the control input, making the constraint enforceable via a first-order condition. The energy-based safety function is given by [10]:

$$h_D = -\frac{1}{2}\dot{q}^{\mathrm{T}}\mathrm{M}\dot{q} + \alpha_e h \tag{7}$$

The corresponding energy-based safe set is defined as [10]:

$$S_D = \{(q, \dot{q}) \in \mathcal{Q} \times \mathbb{R}^k : h_D(q, \dot{q}) \geq 0\} \tag{8}$$

Here, $S_D \subseteq S$, and the parameter α_e modulates the conservativeness of the safe set. A larger α_e results in a set S_D that more closely approximates the original safe set S. To ensure constraint satisfaction, the nominal control input F_{des} is minimally adjusted using a Quadratic Program (QP) [10].

Definition 2. *For a fully-actuated robotic system governed by the dynamics in* (2)*, assume a position safety constraint h defines a corresponding set S as in* (5)*. Let h_D denote the energy-based safety function, inducing a safe set S_D defined in* (8)*. A control policy that ensures safety over the set S_D is given by:*

$$\begin{aligned} \mathrm{F}^* = \arg\min_{\mathrm{F} \in \mathbb{R}^m} \|\mathrm{F} - \mathrm{F}_{des}\|^2 \\ \text{s.t.} \quad \underbrace{-\dot{q}^{\mathrm{T}}\mathrm{HF} + \mathrm{G}(q)^{\mathrm{T}}\dot{q} + \alpha_e \dot{h}}_{\dot{h}_D(q,\dot{q},\mathrm{F})} \geq -\alpha(h_D(q, \dot{q})) \end{aligned} \tag{9}$$

A closed-form solution to this QP can also be derived by considering the Karush-Kuhn-Tucker (KKT) conditions [10], [27]:

$$\mathrm{F}^* = \mathrm{F}_{des} + \begin{cases} \frac{\mathrm{H}^{\mathrm{T}}\dot{q}}{\|\mathrm{H}^{\mathrm{T}}\dot{q}\|^2}\Psi, & \Psi < 0 \\ 0, & \Psi \geq 0 \end{cases} \tag{10}$$

and the safety violation term Ψ is defined by:

$$\Psi = \dot{h}_D + \alpha(h_D(q, \dot{q})) \tag{11}$$

Where $\alpha(h_D(q, \dot{q})) = \alpha h_D$. This formulation allows the use of relative-degree-one CBF conditions on second-order systems without requiring higher-order Lie derivatives.

D. Velocity CBF

In addition to enforcing position safety, velocity constraints are essential due to the platform's limited workspace. To address this, we introduce a velocity-based CBF that directly constrains the system's velocity. Let the velocity CBF be defined as $h_v(\dot{q})$, which is a function that take the system's velocity as an input. Since h_v has relative degree one, its derivative includes the control input and allows direct enforcement through a standard CBF formulation. The first-time derivative of h_v is then defined as $\dot{h}_v$

Definition 3. *Consider a robotic system governed by the dynamics in* (2)*. Let h_v be a velocity-based safety constraint. A controller that ensures forward invariance of the associated safe set can be synthesized using:*

$$\begin{aligned} \mathrm{F}^* = \arg\min_{\mathrm{F} \in \mathbb{R}^m} \|\mathrm{F} - \mathrm{F}_{des}\|^2 \\ \text{s.t.} \quad \dot{h}_v \geq -\alpha(h_v(\dot{q})) \end{aligned} \tag{12}$$

The corresponding closed-form solution of (12) is defined by the following:

$$\mathrm{F}^* = \mathrm{F}_{des} + \begin{cases} \frac{\mathrm{M}^{-1}\mathrm{H}}{\|\mathrm{M}^{-1}\mathrm{H}\|^2}\Psi_v, & \Psi_v < 0 \\ 0, & \Psi_v \geq 0 \end{cases} \tag{13}$$

while the safety violation term Ψ_v is defined by:

$$\Psi_v = \dot{h}_v + \alpha_v(h_v) \tag{14}$$

where $\alpha_v(h_v) = \alpha_v h_v$.

III. System Framework and Problem Formulation

To ensure safety in both position and velocity states, the corresponding constraints must be integrated into the control formulation. For QP-based CBFs, this integration is straightforward: the constraints are stacked into a single inequality, and the solver handles them jointly. However, in a closed-form setting, incorporating both requires analyzing

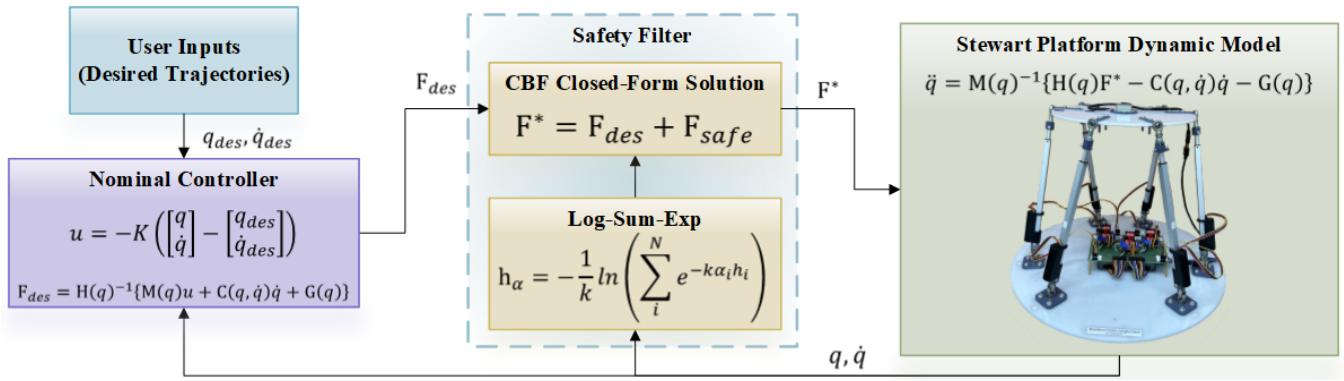

Fig. 2. The architecture of the proposed Stewart platform controller.

multiple KKT conditions and resolving the interaction between distinct safety constraints analytically. Moreover, due to the multiple DoF that the Stewart platform system has, it is important to ensure safety specifications across multiple axes. We define the problem statement as follows:

Problem III.1. *Given the Stewart platform dynamics in* (2)*, derive a closed-form Control Barrier Function (CBF) that enforces both position and velocity safety constraints, based on the quadratic programming formulations in* (9) *and* (12)*. The formulation should also accommodate the use of different CBF parameters across constraints, enabling resolution of conflicting safety requirements.*

In response to Problem III.1, we propose a Stewart platform controller architecture as shown in Fig. 2. We present two contributions: (1) a closed-form solution that simultaneously enforces position and velocity safety, and (2) flexible CBF parameter tuning across conflicting constraints.

IV. Closed-Form CBF for Position and Velocity Safety

To address Problem III.1, we aim to construct a controller that ensures both position and velocity safety. This is formulated as a QP that combines both position and velocity constraints from (9) and (12):

$$\begin{aligned} \mathrm{F}^* &= \arg\min_{\mathrm{F}\in\mathbb{R}^m} \|\mathrm{F} - \mathrm{F}_{des}\|^2 \\ \text{s.t.} \quad & \underbrace{-\dot{q}^{\mathrm{T}}\mathrm{HF} + \mathrm{G}(q)^{\mathrm{T}}\dot{q} + \alpha_e \dot{h}}_{\dot{h}_D(q,\dot{q},\mathrm{F})} \geq -\alpha(h_D(q,\dot{q})) \\ & \underbrace{-(\mathrm{M}^{-1}(\mathrm{H}(q)\mathrm{F} - \mathrm{C}(q,\dot{q})\dot{q} - \mathrm{G}(q)))}_{\dot{h}_v(\dot{q},\mathrm{F}_{des})} \geq -\alpha_v(h_v(\dot{q})) \end{aligned} \tag{15}$$

To avoid solving the QP online at every time step, we derive an explicit closed-form controller using the KKT conditions. The resulting controller behaves in a piecewise function, depending on which constraints are active: If no constraint is active, the controller applies the nominal input F_{des}. If only one constraint (either position or velocity) is active, the corresponding single constraint solution from (10) or (13) is used. If both constraints are active, the following closed-form control law is applied:

$$\mathrm{F}^* = \mathrm{F}_{des} - \frac{1}{2}\left(\lambda_1 \left(\mathrm{H}^{\mathrm{T}}\dot{q}\right)^{\mathrm{T}} + \lambda_2 \left(\mathrm{M}^{-1}\mathrm{H}\right)^{\mathrm{T}}\right) \tag{16}$$

$a_2 =$ are the control-dependent terms introduced in (10) and (13), respectively. Moreover, λ_1 and λ_2 are the Lagrange multipliers associated with the position and velocity constraints, respectively. These are obtained by solving the following linear system:

$$\begin{bmatrix} \lambda_1 \\ \lambda_2 \end{bmatrix} = \begin{bmatrix} \frac{1}{2}\| \mathrm{H}^{\mathrm{T}}\dot{q}\|^2 & \frac{1}{2}\left(\mathrm{H}^{\mathrm{T}}\dot{q}\right)\left(\mathrm{M}^{-1}\mathrm{H}\right)^{\mathrm{T}} \\ \frac{1}{2}\left(\mathrm{M}^{-1}\mathrm{H}\right)\left(\mathrm{H}^{\mathrm{T}}\dot{q}\right)^{\mathrm{T}} & \frac{1}{2}\|\mathrm{M}^{-1}\mathrm{H}\|^2 \end{bmatrix}^{-1} \begin{bmatrix} -\Psi \\ -\Psi_v \end{bmatrix} \tag{17}$$

with Ψ and Ψ_v defined in (11) and (14), respectively. Once λ_1 and λ_2 are computed, they are substituted into (18) to compute the final control input.

Theorem 1. *Consider a fully-actuated robotic system with a dynamic model described by* (2)*. Let h and h_v be the safety constraints for the position and velocity of the system. Then, the control input that enforces both constraints is given by* $\mathrm{F}^* = \mathrm{F}_{des} + \mathrm{F}_{safe}$*, where:*

$$\mathrm{F}_{safe} = \begin{cases} \frac{a_1}{\|a_1\|^2}\Psi, & \Psi < 0, \Psi_v \geq 0 \\ \frac{a_2}{\|a_2\|^2}\Psi_v, & \Psi \geq 0, \Psi_v < 0 \\ -\frac{1}{2}(\lambda_1 a_1^{\mathrm{T}} + \lambda_2 a_2^{\mathrm{T}}), & \Psi \textit{ and } \Psi_v < 0 \\ 0, & \Psi \textit{ and } \Psi_v \geq 0 \end{cases} \tag{18}$$

This piecewise formulation ensures safety by modifying the nominal control input only when a constraint is at risk of being violated. It should be noted that the closed-form solution defined in (18) only considers *one* position constraint and *one* velocity constraint.

Proof: We begin by applying KKT conditions to the QP in (15) with two inequality constraints, denoted c_1 and c_2. The Lagrangian is:

$$\begin{aligned} \mathcal{L} &= \|\mathrm{F} - \mathrm{F}_{des}\|^2 + \lambda_1 c_1 + \lambda_2 c_2 \\ &= (\mathrm{F} - \mathrm{F}_{des})^{\mathrm{T}}(\mathrm{F} - \mathrm{F}_{des}) + \lambda_1 c_1 + \lambda_2 c_2 \end{aligned} \tag{19}$$

The KKT conditions are [28]:

$$\begin{aligned} \text{Stationarity:} \quad & \nabla\mathcal{L} = 0 \\ \text{Dual feasibility:} \quad & \lambda_1, \lambda_2 \geq 0 \\ \text{Primal feasibility:} \quad & c_1, c_2 \leq 0 \\ \text{Complementary slackness:} \quad & \lambda_i c_i = 0 \end{aligned}$$

Each constraint $c_i \leq 0$ is defined as $a_i \mathrm{F} - b_i \leq 0$, where, in the context of the CBF inequality defined in (6), a_i corresponds to the Lie derivative $-Lgh(x)$ term, while b_i corresponds to the $\alpha(h(x)) + Lfh(x)$. Solving the stationarity condition yields:

$$\nabla\mathcal{L} = 2(\mathrm{F}^* - \mathrm{F}_{des}) + \lambda_1 a_1^{\mathrm{T}} + \lambda_2 a_2^{\mathrm{T}} = 0 \tag{20}$$

Next, we solve for F:

$$\mathrm{F}^* = \mathrm{F}_{des} - \frac{1}{2}(\lambda_1 a_1^{\mathrm{T}} + \lambda_2 a_2^{\mathrm{T}}) \tag{21}$$

We now consider the cases based on which constraints are active.

*a) **Case 1—No active constraints**:* This means $\lambda_1 = \lambda_2 = 0$. Substituting into the expression above:

$$\mathrm{F}^* = \mathrm{F}_{des} \tag{22}$$

This corresponds to the case where no safety intervention is required.

*b) **Case 2—Only one constraint is active**:* Suppose only constraint c_i is active (where i is 1 or 2). The stationarity condition becomes:

$$\mathrm{F}^* = \mathrm{F}_{des} - \frac{\lambda_i a_i^{\mathrm{T}}}{2} \tag{23}$$

Substituting this expression into the active constraint $c_i = a_i \mathrm{F}^* - b_i = 0$ gives:

$$a_i(\mathrm{F}_{des} - \frac{\lambda_i a_i^{\mathrm{T}}}{2}) - b_i = 0 \tag{24}$$

Solving for λ_i, we obtain:

$$\lambda_i = -\frac{2(b_i - a_i \mathrm{F}_{des}) a_i^{\mathrm{T}}}{\|a_i\|^2} \tag{25}$$

Substituting this back into (23):

$$\mathrm{F}^* = \mathrm{F}_{des} + \frac{(b_i - a_i \mathrm{F}_{des}) a_i^{\mathrm{T}}}{\|a_i\|^2} \tag{26}$$

This corresponds to the closed-form solution when only one safety constraint is active. Since it considers two constraints, it produces two cases in which one of the constraint is active when the other is not.

*c) **Case 3—Both constraints are active**:* We substitute (21) into both constraints:

$$\begin{aligned} a_1(\mathrm{F}_{des} - \frac{1}{2}(\lambda_1 a_1^{\mathrm{T}} + \lambda_2 a_2^{\mathrm{T}})) - b_1 = 0 \\ a_2(\mathrm{F}_{des} - \frac{1}{2}(\lambda_1 a_1^{\mathrm{T}} + \lambda_2 a_2^{\mathrm{T}})) - b_2 = 0 \end{aligned} \tag{27}$$

This results in a system of two linear equations in λ_1 and λ_2, which can be solved analytically. The solution corresponds to (17), and the multipliers are substituted back into the expression (21) to yield the final control law.

Corollary 1. *The CBFs defined in* (18) *only considers one position and velocity constraint. To enforce multiple constraint, they functions can be combined using a smooth* min *approximation via the Log-Sum-Exp (LSE) function:*

$$\begin{aligned} h_{pos} &= -\frac{1}{k} ln(\sum_{i=1}^{N} e^{-k h_{Di}}) \\ h_{vel} &= -\frac{1}{k} ln(\sum_{i=1}^{N} e^{-k h_{vi}}) \end{aligned} \tag{28}$$

where $k > 0$ controls the smoothness of the approximation, h_{Di} denotes the i-th energy-based position constraint, and h_{vi} denotes the i-th velocity constraint.

Due to the combined constraints, the closed-form solution defined in (18) is also changing. The derivation steps are the same, with the only change are with the h and $\dot{h}$. The inequality constraints defined in (15) is then changed into the following:

$$\begin{aligned} \dot{h}_{pos} &\geq -\alpha(h_{pos}) \\ \dot{h}_{vel} &\geq -\alpha_v(h_{vel}) \end{aligned} \tag{29}$$

where $\dot{h}_{pos}$ and $\dot{h}_{vel}$ are the first-time derivatives of the respective functions. Thus, the closed-form solution, while the take the same derivation steps as shown in the proof, is defined as $\mathrm{F}^* = \mathrm{F}_{des} + \mathrm{F}_{safe}$, where:

$$\mathrm{F}_{safe} = \begin{cases} \frac{a_p}{\|a_p\|^2}\Psi, & \Psi < 0, \Psi_v \geq 0 \\ \frac{a_v}{\|a_v\|^2}\Psi_v, & \Psi \geq 0, \Psi_v < 0 \\ -\frac{1}{2}(\lambda_1 a_p^{\mathrm{T}} + \lambda_2 a_v^{\mathrm{T}}), & \Psi \text{ and } \Psi_v < 0 \\ 0, & \Psi \text{ and } \Psi_v \geq 0 \end{cases} \tag{30}$$

where

$$\begin{aligned} a_p &= \sum_{i=1}^{N} w_{pi} a_i \\ a_v &= \sum_{i=1}^{N} w_{vi} a_i \end{aligned} \tag{31}$$

and the weights are defined by

$$\begin{aligned} w_{pi} &= e^{(h_{Di} - h_{vel})} \\ w_{vi} &= e^{(h_{vi} - h_{vel})} \end{aligned} \tag{32}$$

Remark 1. *To allow different safety–performance trade-offs for each constraint, we introduce an α-weighted LSE:*

$$\begin{aligned} h_{pos} &= -\frac{1}{k} ln(\sum_{i=1}^{N} e^{-k \alpha_i h_{Di}}) \\ h_{vel} &= -\frac{1}{k} ln(\sum_{i=1}^{N} e^{-k \alpha_{vi} h_{vi}}) \end{aligned} \tag{33}$$

where α_i and α_{vi} are positive scaling parameters for the i-th position and velocity constraints, respectively. The closed-form CBF formulation is still following the same structure as

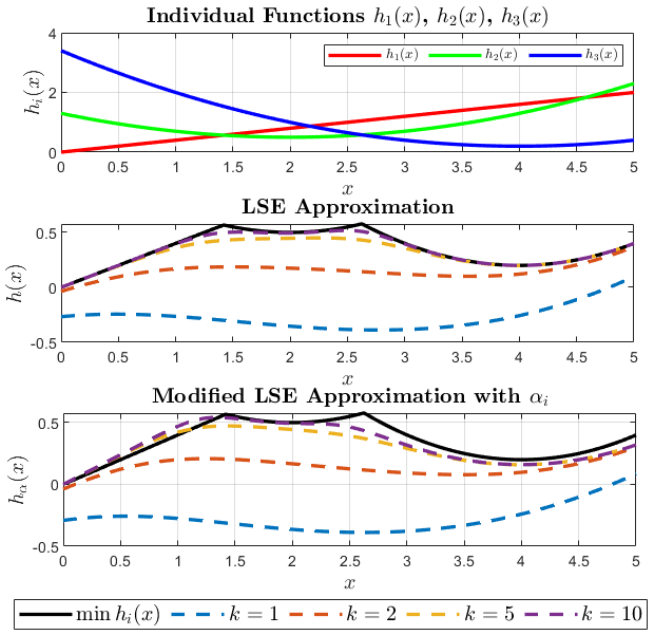

Fig. 3. LSE approximation of a min function.

written in (18). *Due to the inclusion of the CBF parameters within the LSE, the class-$\mathcal{K}$ function for the position and velocity is then defined as* $\alpha(h) = \mathrm{h_{pos}}$ *and* $\alpha_v(h_v) = \mathrm{h_{vel}}$, *respectively. Consequently:*

$$\begin{aligned} \Psi &= \dot{h}_{pos} + h_{pos} \\ \Psi_v &= \dot{h}_{vel} + h_{vel} \end{aligned} \tag{34}$$

As an example, consider three different functions, defined by $h_i(x)$ where $i = 1, 2, 3$. The objective is to find the minimum values across all x values using the modified LSE method. et $k = 1, 2, 5, 10$ and $\alpha_1 = 1.2$, $\alpha_2 = 1$, $\alpha_3 = 0.8$ for each corresponding functions. The result of the example is shown in Fig. 3. The real minimum values of the three functions are denoted with the black solid line. The figure shows the result of the original and the proposed LSE. The example shows that with the proposed LSE, the parameter α_i can influence the approximation, making each constraint more prone to violating or making it more conservative. In turn, it will make the safety filter much more sensitive or relaxed to the constraint violations, depending on the α_i value correlated to the individual constraints.

As an illustrative case, we consider the enforcement of multiple safety constraints on the Stewart platform. The platform is set reach a desired linear positions near the bounds. Using the original LSE with uniform CBF parameters ($\alpha = \alpha_e = \alpha_v = 1$), the results reveal conflicting constraints along the Z-axis, manifested as fluctuations in the actuator forces (Fig. 4). In contrast, our proposed weighted LSE formulation incorporates distinct CBF parameters within the LSE. By assigning $\alpha = 10$ and $\alpha_v = 0.5$ for the Z-axis constraints, the resulting safety filter generates smoother force profiles and maintains steady Z-axis velocity, demonstrating improved stability of the control inputs.

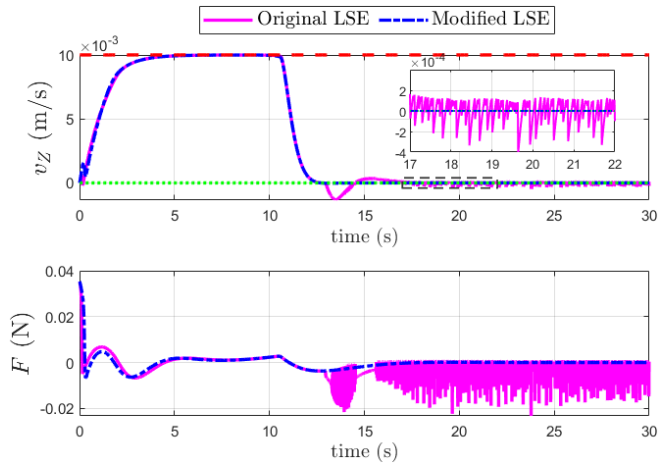

Fig. 4. Comparison between the original and modified LSE.

V. Simulation and Experiment Results

A Stewart platform prototype was developed for real-world experiments using a combination of off-the-shelf and custom-fabricated components. The prototype was made by considering the production cost and potential research capabilities. The platform's legs are driven by six Actuonix P-16P linear actuators with built-in potentiometer feedback, allowing precise length control based on platform state measurements. Additionally, an IMU sensor provides accurate measurements of the platform's angular motion, complementing the potentiometer feedback from the actuators. A National Instruments (NI) myRIO-1900 embedded real-time controller, programmed in LabVIEW, manages data acquisition and control: it receives sensor readings and sends actuation commands through motor drivers. Structural components such as the platform, base, and joint connectors were custom-designed in CAD to match the actuator geometry, with the platform and base laser-cut from 5 mm acrylic and the joint connectors 3D-printed from a durable material. The platform has a real radius (the physical acrylic disk radius) and an effective radius (distance from frame origin to the joints), the latter determined by joint placement. Hardware specifications of the prototype are summarized in I, and the assembled prototype is shown in Fig. 1(b).

This section presents simulation and experimental results to evaluate the the proposed methods in enforcing safety constraints while maintaining system performance on the Stewart platform. The analysis focuses on the role of CBFs in regulating motion and ensuring stability under multiple simultaneous constraints. The simulation results compare the closed-form and QP-based implementations of CBFs, highlighting their respective abilities to enforce safety and influence system behavior, while also showing the advantages that the closed-form solution offers in terms of computational loads. In addition to that, the experimental results compare the two CBF methods when applied to the Stewart platform prototype.

A. Scenario and Parameter Setup

For the simulations and experiments, initial condition of the platform is set to the following states:

$$q_0 = [0, 0, 0.4, 0, 0, 0]^{\mathrm{T}}, \quad \dot{q}_0 = [0, 0, 0, 0, 0, 0]^{\mathrm{T}} \tag{35}$$

where q_0 and $\dot{q}_0$ are the initial position and velocity, respectively. The constraints are only applied for the upper position and velocity of the platform. The position constraints are defined by $h_X = h_Y = 0.11\mathrm{m}$, $h_Z = 0.51\mathrm{m}$. Meanwhile, the veloctiy constraints are defined by $h_{vX} = h_{vY} = 15 \times 10^{-3}\mathrm{m/s}$, $h_{vZ} = 10 \times 10^{-3}\mathrm{m/s}$.

The platform is commanded to move along all three translational axes. It evaluates the combined position and velocity constraint enforcement capability of the proposed CBF method and demonstrates the effectiveness of the proposed smooth approximation used in the closed-form solution. The platform is required to achieve and maintain a sequence of distinct static poses as defined below:

$$\begin{aligned} q_{des} &= [X_{des}, Y_{des}, Z_{des}, \phi_{des}, \theta_{des}, \psi_{des}]^{\mathrm{T}} \\ \dot{q}_{des} &= [0, 0, 0, 0, 0, 0]^{\mathrm{T}} \end{aligned} \tag{36}$$

Each component of q_{des} follows a piecewise function defined as:

$$\begin{aligned} X_{des} &= \begin{cases} 0.1, & \text{if } 0 \le t < 10 \\ 0, & \text{otherwise} \end{cases} \\ Y_{des} &= \begin{cases} 0.1, & \text{if } 10 \le t < 20 \\ 0, & \text{otherwise} \end{cases} \\ Z_{des} &= \begin{cases} 0.45, & \text{if } 20 \le t < 30 \\ 0.5, & \text{if } 30 \le t < 40 \\ 0.4, & \text{otherwise} \end{cases} \end{aligned} \tag{37}$$

B. Simulation Result and Discussion

Simulations compared the Stewart platform's response under two CBF implementations: a closed-form solution and a QP-based formulation. Both used identical parameters ($\alpha = \alpha_e = \alpha_v = 1$) except for the Z-axis velocity constraint, where $\alpha_v = 2$. Figure 5 shows position, velocity, and computation time for all axes.

TABLE I

STEWART PLATFORM PARAMETERS

Component	Specifications
Embedded Device	NI myRIO-1900
Platform and Base	Custom-cut acrylic with 5 mm thickness Real base radius: 30 cm Effective base radius: 20 cm Real platform radius: 15 cm Effective platform radius: 16 cm
Motor Drivers	L298N Motor Driver
Actuators	Actuonix P-16P Linear Actuator with potentiometer feedback and 20 cm stroke
Platform joint	PHS5 Rod-End Bearing
Base joints	Universal joint Inner hole diameter: 10 mm Outer diameter: 16 mm
IMU Sensor	Hfi-b9 ROS IMU Module

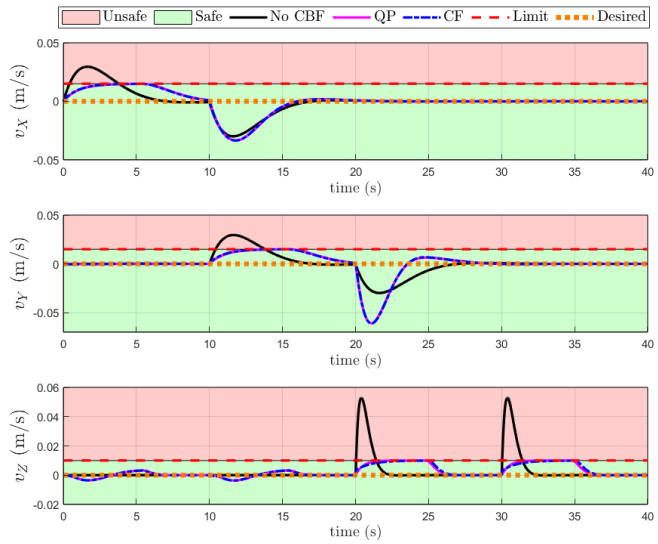

Fig. 5. Simulation results of the proposed controller that is implemented on the Stewart platform system.

Both controllers maintained safety across all axes with similar tracking accuracy. Differences emerged when multiple constraints were active, particularly in the Z-axis where enforcing X and Y constraints induced unintended Z motion due to dynamic coupling. Once X and Y constraints were relaxed, Z tracking recovered. Performance-wise, both method yielded similar results, which validate the closed-form solution of the proposed controller.

The main distinction lies in computation time: the closed-form method averaged 1.6016×10^{-4} seconds per iteration, versus 0.0061 seconds for the QP. The closed-form approach computation time is about 38 times faster than the QP, which validate the fact that the closed-form method requires less computational time.

C. Experiment Results and Discussion

Experiments on the Stewart platform prototype used the same scenarios and constraints as in simulation, ensuring consistent evaluation. Full-state feedback was provided, with an Extended Kalman Filter for state estimation. The CBF parameters matched the simulation, except for the Z-axis velocity constraint (α_v increased from 2 to 100) to improve enforcement under unmodeled real-world effects.

Figure 6 compares the operation with and without the proposed CBF. The controller successfully enforced multiple constraints, maintaining operation within safety limits. The computational time of the QP method averaged 2.4×10^{-3} seconds per iteration, while the closed-form averaged 4.40×10^{-4} seconds. It makes the closed-from method about 5.4 times faster and it avoided the large time spikes seen in the QP during constraint violations.

VI. CONCLUSIONS

This paper presented a CBF controller to ensure both position and velocity safety for a Stewart platform. Simulation results demonstrated that the proposed controller

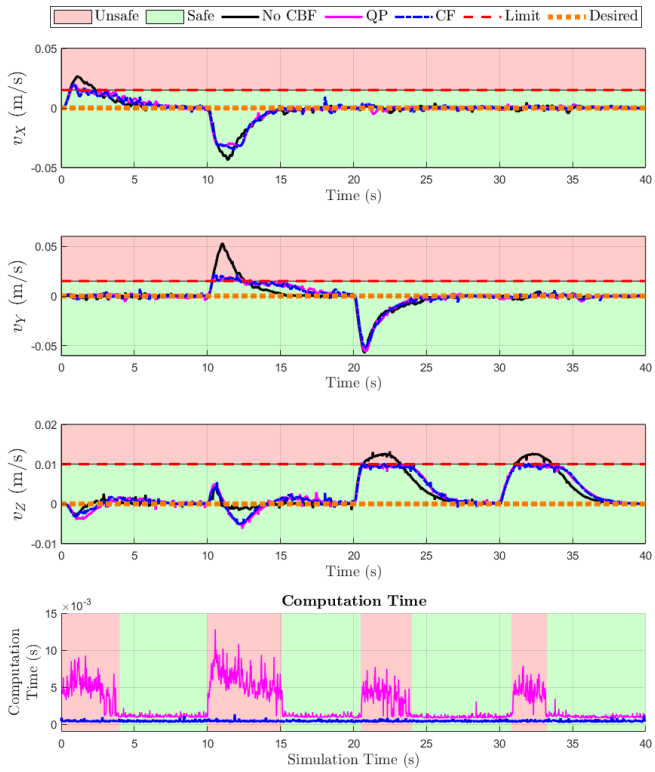

Fig. 6. Comparisson of experimental results of the with and without proposed CBF.

successfully enforces safety constraints, while also validating the use of the modified LSE method for approximating the $\min$ function to combine multiple constraints. Although differences were observed between the QP-based and closed-form implementations, as well as between simulation and experiment, these are attributed to unmodeled dynamics, parameter tuning differences, and sensor noise in real-world settings. Despite these variations, the experimental results confirm that the proposed controller effectively guarantees safe operation of the Stewart platform prototype.

Future work will explore the integration of control input constraints into the closed-form framework. Additionally, adaptive CBF formulations that can handle model uncertainty and external disturbances, as well as configuring conservativeness of the safety will be investigated to improve robustness and generalizability.

References

[1] A. D. Ames, S. Coogan, M. Egerstedt, G. Notomista, K. Sreenath, and P. Tabuada, "Control barrier functions: Theory and applications," in *2019 18th European control conference (ECC)*, pp. 3420–3431, Ieee, 2019.

[2] K. Garg, J. Usevitch, J. Breeden, M. Black, D. Agrawal, H. Parwana, and D. Panagou, "Advances in the theory of control barrier functions: Addressing practical challenges in safe control synthesis for autonomous and robotic systems," *Annual Reviews in Control*, vol. 57, p. 100945, 2024.

[3] T. G. Molnar and A. D. Ames, "Composing control barrier functions for complex safety specifications," *IEEE Control Systems Letters*, vol. 7, pp. 3615–3620, 2023.

[4] A. Cristofaro, M. Ferro, and M. Vendittelli, "Safe trajectory tracking using closed-form controllers based on control barrier functions," in *2022 IEEE 61st Conference on Decision and Control (CDC)*, pp. 3329–3334, IEEE, 2022.

[5] C. K. Verginis and D. V. Dimarogonas, "Closed-form barrier functions for multi-agent ellipsoidal systems with uncertain lagrangian dynamics," *IEEE Control Systems Letters*, vol. 3, no. 3, pp. 727–732, 2019.

[6] Q. Nguyen and K. Sreenath, "Exponential control barrier functions for enforcing high relative-degree safety-critical constraints," in *2016 American Control Conference (ACC)*, pp. 322–328, IEEE, 2016.

[7] W. Xiao and C. Belta, "High-order control barrier functions," *IEEE Transactions on Automatic Control*, vol. 67, no. 7, pp. 3655–3662, 2021.

[8] T. G. Molnar and A. D. Ames, "Safety-critical control with bounded inputs via reduced order models," *arXiv preprint arXiv:2303.03247*, 2023.

[9] S. Kolathaya, "Energy based control barrier functions for robotic systems," *Authorea Preprints*, 2023.

[10] A. Singletary, S. Kolathaya, and A. D. Ames, "Safety-critical kinematic control of robotic systems," *IEEE Control Systems Letters*, vol. 6, pp. 139–144, 2021.

[11] Y. Choudhary and S. Kolathaya, "Energy based control barrier functions for robotic manipulators with large safety constraints," in *2022 European Control Conference (ECC)*, pp. 1328–1335, IEEE, 2022.

[12] J. Breeden and D. Panagou, "Compositions of multiple control barrier functions under input constraints," *arXiv preprint arXiv:2210.01354*, 2022.

[13] N. Dini, Y. Batmani, and M. Davoodi, "Closed-form robust safe output-feedback control design for nonlinear systems," *IFAC-PapersOnLine*, vol. 58, no. 28, pp. 498–503, 2024.

[14] C. Wang, X. Wang, Y. Dong, L. Song, and X. Guan, "Multi-constraint safe reinforcement learning via closed-form solution for log-sum-exp approximation of control barrier functions," *arXiv preprint arXiv:2505.00671*, 2025.

[15] J. Ferlez, M. Elnaggar, Y. Shoukry, and C. Fleming, "Shieldnn: A provably safe nn filter for unsafe nn controllers," *arXiv preprint arXiv:2006.09564*, 2020.

[16] P. Rabiee and J. B. Hoagg, "A closed-form control for safety under input constraints using a composition of control barrier functions," *arXiv preprint arXiv:2406.16874*, 2024.

[17] P. Rabiee and J. B. Hoagg, "Composition of control barrier functions with differing relative degrees for safety under input constraints," in *2024 American Control Conference (ACC)*, pp. 3692–3697, IEEE, 2024.

[18] D. Stewart, "A platform with six degrees of freedom," *Proceedings of the Institution of Mechanical Engineers*, vol. 180, no. 1, pp. 371–386, 1965.

[19] W. Qiu, S. Wang, A. Niu, K. Fan, G. Han, and H. Chen, "Modeling and analysis of landing collision dynamics for an active helideck based on the stewart platform," *Ocean Engineering*, vol. 297, p. 117107, 2024.

[20] W. Chen, Y. Wen, X. Tong, C. Lin, J. Li, S. Wang, W. Xie, L. Mao, X. Zhao, W. Zhang, *et al.*, "Dynamics modeling and modal space control strategy of ship-borne stewart platform for wave compensation," *Journal of Mechanisms and Robotics*, vol. 15, no. 4, p. 041015, 2023.

[21] S. Kizir and Z. Bingül, "Design and development of a stewart platform assisted and navigated transsphenoidal surgery," *Turkish Journal of Electrical Engineering and Computer Sciences*, vol. 27, no. 2, pp. 961–972, 2019.

[22] F. Liang, S. Tan, X. Zhao, J. Fan, Z. Lin, Z. Shi, and X. Kang, "Kinematics and dynamics simulation of a stewart platform," in *Journal of Physics: Conference Series*, vol. 2333, p. 012026, IOP Publishing, 2022.

[23] G. Kazezkhan, Q. Xu, N. Wang, F. Xue, and H. Wang, "Performance analysis and optimization of a modified stewart platform for the qitai radio telescope," *Research in Astronomy and Astrophysics*, vol. 23, no. 9, p. 095022, 2023.

[24] H. Guo and H. Li, "Dynamic analysis and simulation of a six degree of freedom stewart platform manipulator," *Proceedings of the IMechE, Part C: J. Mech. Eng. Sci.*, vol. 220, no. 1, pp. 61–72, 2006.

[25] A. Şumnu, İ. H. Güzelbey, and M. V. Çakir, "Simulation and pid control of a stewart platform with linear motor," *Journal of mechanical science and technology*, vol. 31, pp. 345–356, 2017.

[26] Z. Bingul and O. Karahan, "Dynamic modeling and simulation of stewart platform, serial and parallel robot manipulators–kinematics,

dynamics, control and optimiziation, ed. by s. kucuk, publisher in tech," *Serial and Parallel Robot Manipulators*, 2012.

[27] H. Wang, K. Margellos, and A. Papachristodoulou, "Explicit solutions for safety problems using control barrier functions," in *2022 IEEE 61st Conference on Decision and Control (CDC)*, pp. 5680–5685, IEEE, 2022.

[28] J. Nocedal and S. J. Wright, *Numerical optimization*. Springer, 2006.